THE JOURNAL OF PHYSICAL CHEMISTRY Letters

Letter

pubs.acs.org/JPCL

Ultrafast Transient Absorption Spectroscopy of the Sunscreen Constituent Ethylhexyl Triazone

Lewis A. Baker,*[,†,‡] Sarah L. Clark,[†] Scott Habershon,[†,‡] and Vasilios G. Stavros*[,†]

[†]Department of Chemistry and [‡]Centre for Scientific Computing, University of Warwick, Gibbet Hill Road, Coventry CV4 7AL, United Kingdom

Supporting Information

ABSTRACT: The ultrafast photoprotection mechanisms in operation in ethylhexyl triazone (EHT, octyl triazone), an approved ultraviolet-B (UV-B) chemical filter for commercial sunscreens, remain elusive, with a notable absence of ultrafast time-resolved measurements. These large organic molecules are of increasing interest as they are suspected to be less likely to penetrate the skin than some of the smaller approved filters, thereby reducing the possible adverse effects from sunscreen products. We apply femtosecond transient absorption spectroscopy with electronic structure calculations to unravel the complete photodeactivation mechanism that EHT undergoes after UV-B irradiation. We propose that this involves ultrafast internal conversion of the initially photoexcited $n^1\pi\pi^*$ state that couples to the ground state via a $1^1\pi\pi^*/S_0$ conical intersection, enabling multiple absorption and recovery cycles, as one would anticipate from a highly efficient filter. We also observe long-lived photoproducts which, based on previous studies along with present electronic structure calculations, we attribute to trapped excited populations in the S_1 and T_1 states.

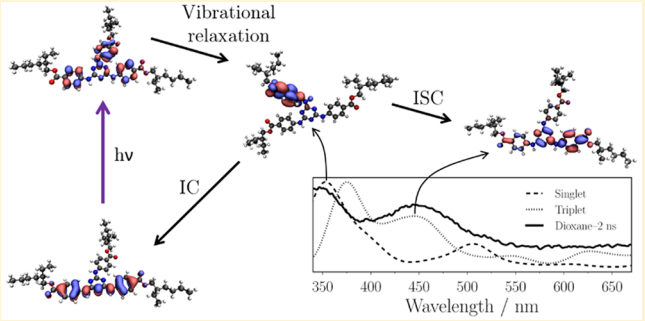

INTRODUCTION

Sunscreens preemptively protect the skin from the damaging effects of overexposure to ultraviolet (UV) radiation.[1] Even though the damaging effects of UV overexposure, specifically by the UV-B region (280−315 nm), have been known for some time,[2] malignant melanoma rates and other UV-related illnesses are on the rise and contribute quite significantly to the global disease burden.[3−5] Given the current trends of increased sun exposure, particularly in the travel and tourism scene,[6] sunscreen safety and regulation is constantly being scrutinized.[7−10] One area of scrutiny surrounds the absorption and recovery cycle of organic chemical filters, which are common constituents of sunscreen products and of which there are many currently approved around the world.[11]

From a photophysical and photochemical point-of-view, an evaluation of such absorption and recovery cycles can be addressed through the measurement of steady-state properties, such as absorption, fluorescence, phosphorescence, and photostability/photodegradation studies. However, from these studies alone, it is often difficult, or indeed impossible, to determine the photodeactivation mechanism(s) in operation. Transient absorption spectroscopy has proven to be a valuable tool in measuring and analyzing such mechanisms on femtosecond to picosecond time scales, with a growing application toward sunscreens.[5,12,13]

In this study we focus on one organic filter,[11,13] ethylhexyl triazone (octyl triazone; termed EHT hereon, see inset of Figure 1). It is one of many organic filters authorized for use across Europe, Australia, New Zealand, Japan, and South Africa,[11] and resembles a group of large aromatic organic filters that are also used in sunscreens such as bis-ethylhexyloxyphenol methoxyphenyl triazine (bemotrizinol) and diethylhexyl butamido triazone (iscotrizinol).[11] A particularly interesting property of EHT (and the family in general) is its large molecular weight (823.07 g·mol^{-1}); such filters are unlikely to penetrate the skin, thereby reducing effects associated with such skin penetration.[15] It displays a broad absorption profile across the UV-B region, with a maximum absorption at ∼311 and ∼313 nm for EHT−dioxane and EHT−methanol, respectively (see Figure 1). Much work has been focused on EHT from a photostability viewpoint, where it is generally regarded as photostable,[16,17] although under certain conditions can photodegrade.[16] Other work has investigated the role EHT plays as a photostabilizer on other organic filters such as avobenzone.[16]

To date, the literature on the ultrafast photochemistry of EHT remains sparse compared with other common organic filters,[12] with most studies involving EHT focusing on its photostability[16,17] and photoallergy properties.[18] Recent work by Tsuchiya et al.[19] has examined the excited states of EHT (and a close derivative diethylhexylbutamido triazone) primarily through the use of steady-state techniques including fluorescence and phosphorescence. The reported fluorescence

Received: March 15, 2017
Accepted: April 24, 2017
Published: April 24, 2017

DOI: 10.1021/acs.jpclett.7b00633
J. Phys. Chem. Lett. 2017, 8, 2113−2118

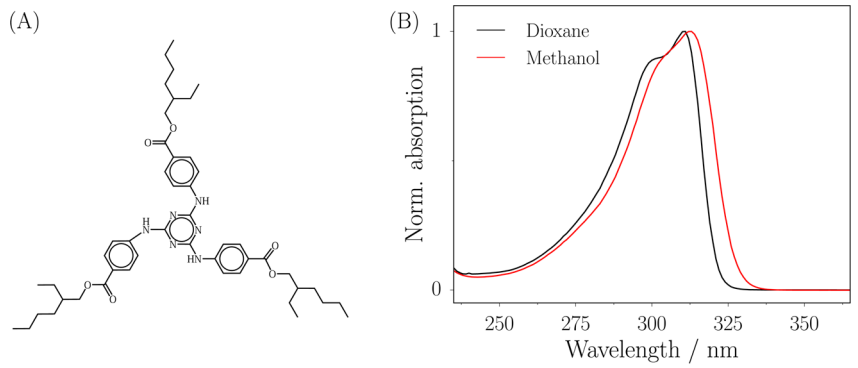

Figure 1. (A) Structure of ethylhexyl triazone (EHT). (B) UV−visible absorption spectrum of EHT−dioxane and EHT−methanol.[14]

and phosphorescence quantum yields at room temperature suggest that internal conversion is the dominant deactivation mechanism after UV photoexcitation. The decay of the fluorescence profile returns a lifetime that is resolution-limited, below 0.6 ns; phosphorescence, on the contrary, decays with a lifetime reported to be several seconds. These results are useful in characterizing the excited states involved in the photodeactivation of EHT; however, the findings also point toward ultrafast processes being involved, something beyond the experimental resolution of the reported study.[19]

It is here where ultrafast spectroscopy can begin to unravel these processes[12] and is the topic of this Letter. We utilize solution-phase transient electronic absorption spectroscopy (TEAS) to probe the photodeactivation mechanism of EHT in the nonpolar solvent dioxane and the polar solvent methanol. Our results agree with previous work,[19] that internal conversion is likely the dominant deactivation mechanism of UV-excited EHT. Initial UV-B photoexcitation to high-lying electronic states results in internal conversion to the first excited electronic state and occurs within ∼400 fs. Following this, a geometry change concomitant with vibrational energy transfer occurs over ∼20 ps, allows population to flow through a conical intersection, and thus repopulate the ground vibrational state of EHT. We also observe the presence of long-lived photoproducts that accord closely with microsecond transient absorption measurements,[19] further evidenced by UV absorption measurements pre- and post-UV-B irradiation, confirming that intersystem crossing to a low-lying triplet state is a likely pathway. The experimental findings observed herein are supported by electronic structure calculations of these photoproducts.

METHODOLOGY

A stock sample of ≥98% EHT was purchased from Sigma-Aldrich and used without further purification. For all reported transient absorption spectra (TAS) measurements, 1 mM solutions of EHT in either dioxane (EHT−dioxane) or methanol (EHT−methanol) were recirculated via a flow-through cell between two CaF_2 windows separated by 100 μm PTFE spacers. Samples were photoexcited by 311 or 313 nm pump-pulses for EHT−dioxane and EHT−methanol, at their respective UV-B absorption maxima, cf. Figure 1B. Pump-pulses with fluences of ∼1 to 2 mJ·cm^{-2} are produced by a commercially available optical parametric amplifier (TOPAS-C, Light Conversion) seeded by a 1 kHz pulse train (1 W, 800 nm) from a Ti:sapphire chirp regenerative amplifier (Spectra-Physics Spitfire Pro XP, 3 W, ∼40 fs). Probe−pulses are derived from a broadband (∼340−670 nm) white-light continuum by focusing a small portion of the 800 nm fundamental (∼5 mW) into a CaF_2 crystal. TAS are collected with the probe−pulse held at the magic angle (54.7°) relative to the pump-pulse, achieved using a half-wave plate in the probe pulse path. All TAS are chirp-corrected using the KOALA package.[20] Further experimental details are provided elsewhere.[21,22]

TAS are analyzed using a global fitting procedure,[23] where the experimental TAS are modeled by the sum of n exponential decay functions, convoluted with a Gaussian instrument response function, $G(\Delta t)$

$$F(\lambda, \Delta t) = \sum_{i}^{n} G(\Delta t) \otimes A_i(\lambda) e^{-(\Delta t - t_0)/\tau_i} \quad (1)$$

where $A_i(\lambda)$ is the decay-associated spectrum (DAS) for the corresponding ith exponential decay function with lifetime τ_i, t_0 denotes the temporal position of pump−probe pulse overlap, and Δt is the pump−probe time delay. The sum of squares between the modeled TAS and experimental TAS is then minimized. $G(\Delta t)$ is a free parameter in eq 1 that is optimized during the fitting procedure; it is, however, restricted to taking a value between 80 and 120 fs based on the typical full width at half-maximum of the instrument response function.[24] Confidence intervals are assigned to reported lifetimes at the 95% level using asymptotic standard errors (see the SI).[25]

All steady-state UV−visible spectroscopic measurements were taken using a Cary 60 UV−visible spectrophotometer with a 1 cm path length quartz cuvette and approximately micromolar EHT−dioxane and EHT−methanol solutions. Continuous-wave UV irradiation studies were performed on EHT to investigate the nature of any long-lived photoproducts using the following procedure. First, a steady-state UV−visible spectrum of each sample was taken to obtain a "before" spectrum. Samples are then irradiated with continuous-wave radiation, ∼50 mW, from an arc lamp (Fluorolog, HORIBA scientific) for 10 min using a central wavelength of 311 or 313 nm (EHT−dioxane and EHT−methanol, respectively) with a bandwidth of ∼5 nm. A second UV−visible spectrum is taken, referred to as the "after" spectrum. Finally, subtraction of the before spectrum from the after spectrum results in the reported "difference spectrum".

RESULTS AND DISCUSSION

Perhaps the most natural place to start is considering the UV−visible spectrum given in Figure 1B. The broad, essentially featureless, nature of the spectrum indicates that a multitude of excited states are accessible in the UV-A and, in particular, the

DOI: 10.1021/acs.jpclett.7b00633
J. Phys. Chem. Lett. 2017, 8, 2113−2118

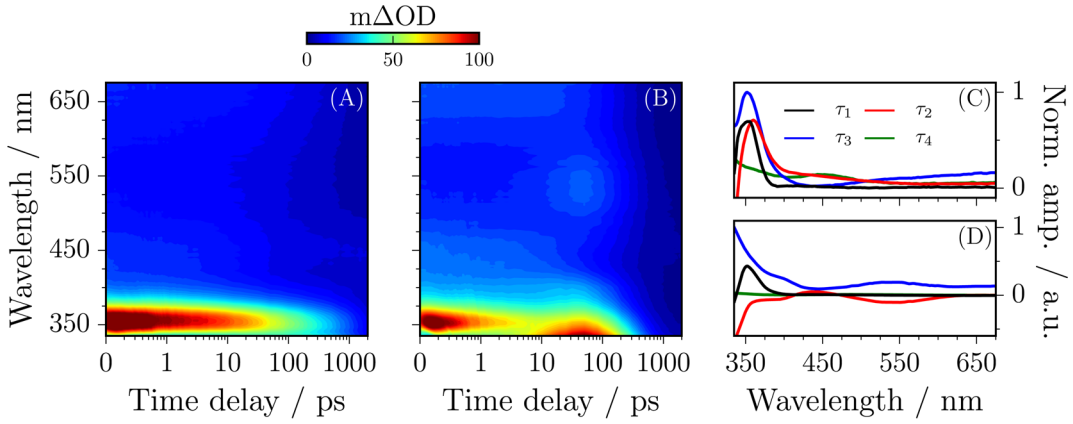

Figure 2. TAS of EHT−dioxane (A) and EHT−methanol (B) shown in the form of a false colormap, where the colors indicate the difference in optical density (ΔOD). The DAS corresponding to the lifetimes of the extracted processes in each TAS are given for EHT−dioxane (C) and EHT−methanol (D). Selected kinetic traces are given in the SI.

UV-B region. Indeed, even at cryogenic temperatures this spectrum remains mostly unchanged.[19] This is further confirmed through density functional theory (vide infra) where ∼20 singlet excited states reside within this broad peak; see Table S1 of the SI

TAS for EHT−dioxane and EHT−methanol photoexcited at 311 and 313 nm, respectively, are shown in Figure 2. Considering EHT−dioxane first (see Figure 2A), the TAS display two main features. The first is an intense absorption centered around probe wavelengths of ∼350 nm. It almost completely decays away by the maximum available pump−probe time delay of 2 ns, indicating that the overall relaxation mechanism in EHT−dioxane predominately is ultrafast, as has been previously suggested.[19] The second is a broad absorption across the rest of the probe window (up to ∼675 nm), which decays toward the baseline, however, not completely, where a clear, broad absorption remains across the probe spectral window, as indicated in Figure 3 (black line).

Quantitative insight into the ultrafast photodeactivation mechanism may be understood by employing a global fitting procedure, as described above.[23] Four exponential functions, convoluted with a Gaussian instrument response function, are required to fully describe the experimental TAS given in Figure 2A. The extracted lifetime for each of these functions is given in Table 1, characterized by its DAS, shown in Figure 2C. The (almost completely) positive nature of each DAS indicates that all extracted lifetimes are associated with decaying features in the TAS. Similar features are observed for EHT−methanol (see Figure 2B) with two differences. The TAS show a signal growing in around 330 nm after ∼10 ps, which then decays away. A broad positive growing signal is also observed centered around 525 nm, which grows in with the signal around 350 nm after $\Delta t \approx 10$ ps. We return to discuss both of these features below. The characteristics of the corresponding DAS corroborate this, where the τ_2 DAS is negative below 350 nm, as well as around 550 nm. This also changes the τ_3 DAS in these regions, given that each lifetime is not sequential in this fitting procedure; each lifetime will capture some of the preceding and proceeding dynamical processes.[26,27] A similar long-lived excited-state profile as seen for EHT−dioxane is observed at the maximum available pump−probe time delay of 2 ns; see Figure 3 (red line).

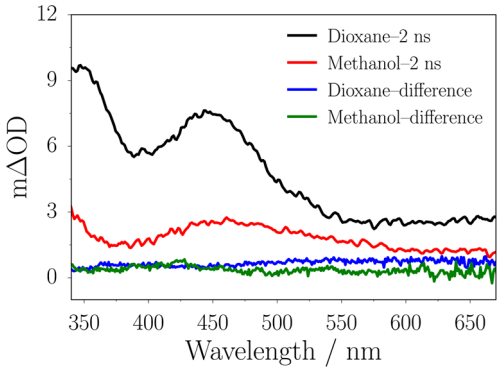

Figure 3. Long-lived signals observed at the maximum pump−probe time delay of 2 ns for EHT−dioxane (black) and EHT−methanol (red). For both systems, very similar spectral features are observed with a peak centered ∼350 and ∼450 nm. Continuous-wave irradiation studies of EHT, resulting in difference spectra (EHT−dioxane, blue; EHT−methanol, green), show flat featureless profiles in contrast with the $\Delta t = 2$ ns spectra.

We first begin discussing these results with reference to the observed long-lived signals in the EHT−dioxane and EHT−methanol TAS at $\Delta t = 2$ ns. The observation of the long-lived feature in both EHT−dioxane and EHT−methanol TAS is explored through the use of continuous UV irradiation. The resulting difference spectrum for each sample is given in Figure 3, calculated after 10 min of irradiation, with the pump wavelength centered on that used in the TEAS studies. Both samples show a flat, almost featureless profile, indicating that there is minimal photoproduct formation; the long-lived signals observed in the TAS must therefore be attributed to metastable transient states. Previous work has shown that photoexcited EHT undergoes both fluorescence and phosphorescence.[19] This work suggested the peak centered around 350 nm might be attributed to excited-state population trapped on the S_1 state

Table 1. Summary of the Lifetimes Extracted from Global Fitting Analysis of the Measured TAS of EHT−Dioxane and EHT−Methanol after UV-B Photoexcitation

lifetime	dioxane	methanol
τ_1/fs	382 ± 33	556 ± 276
τ_2/ps	21.2 ± 2.7	27.9 ± 6.0
τ_3/ps	493.6 ± 68.0	216.0 ± 29.0
τ_4	≫ ns	≫ ns

DOI: 10.1021/acs.jpclett.7b00633
J. Phys. Chem. Lett. 2017, 8, 2113−2118

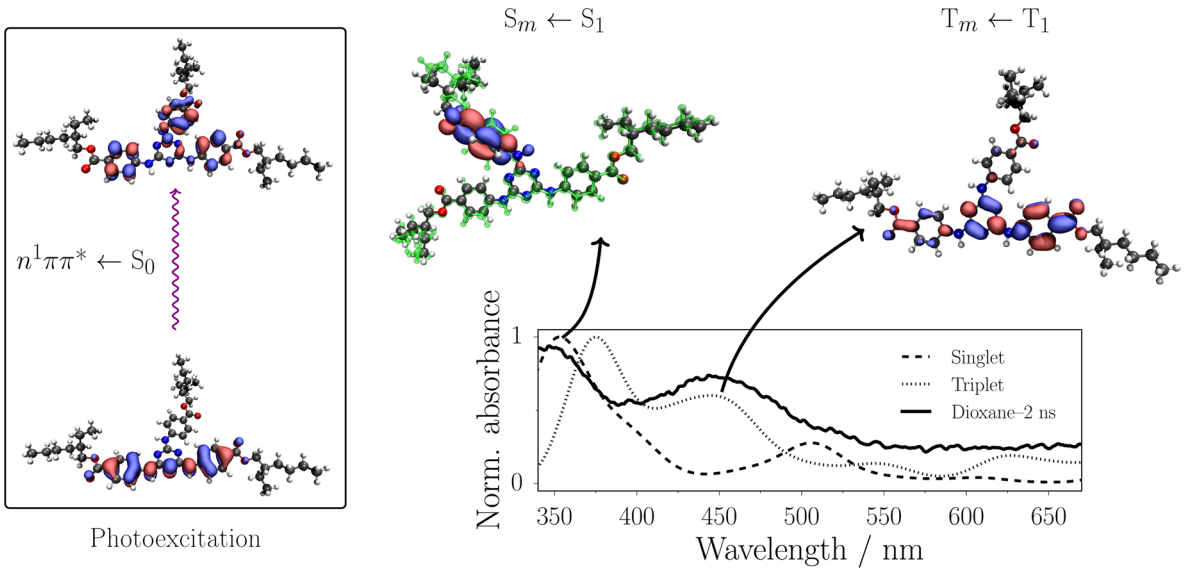

Figure 4. (left) Representative example of the initial photoexcitation, which populates a $n^1\pi\pi^*$ state ($n > 1$, where n refers to the nth singlet excited state; see the SI).[28] (right) The long-lived signal observed for EHT-dioxane at $\Delta t = 2$ ns (black line, cf. Figure 3), the calculated absorption spectrum of the first excited singlet state (dashed line; excited-state geometry shown (opaque) against the ground state geometry (translucent green)), and the first triplet state (short dashed line; excited-state geometry shown). The calculated spectra have been red-shifted by ∼70 nm given the assignment of the experimental ∼450 nm peak to triplet state absorption.[19] Both of these states display significant π character and lead to broad absorption features, suggesting that there is a manifold of accessible excited states ($m \geq 2$) by probe wavelengths.

based on fluorescence measurements. Similarly, the peak centered around 450 nm may be attributed to excited-state population trapped in a triplet state based on phosphorescence and microsecond transient absorption measurements. These, of course, are metastable, and the population would return to the ground S_0 state, the majority of which, however, will be well beyond our maximum experimental pump−probe time delay of 2 ns but before the effective 10 min "time delay" in the continuous-wave measurements.

In an effort to confirm this, electronic structure calculations are performed. We note that these calculations can only provide qualitative support for the experimental results discussed herein. All electronic structure calculations were performed using the TURBOMOLE package.[29,30] Density functional theory and time-dependent density functional theory were used with the BP-86 functional,[31] the augmented Dunning aug-cc-pVDZ basis set,[32,33] the resolution of the identity,[34] and multipole accelerated resolution of the identity approximations,[35] with the corresponding auxiliary basis set.[36] First, the ground-state EHT structure is optimized (see SI for benchmarking with a COSMO implicit solvent[37]), from which vertical excitations suggest that UV-B photoexcitation populates an excited $n^1\pi\pi^*$ state ($n > 1$), where the electronic density remains localized near the central core of EHT; see Figure 4 (left).

We calculate the absorption spectrum of the possible excited-state species. EHT is optimized in its first triplet state, and an array of vertical excitations calculated. The corresponding oscillator strength for each vertical excitation is broadened through convolution with a Gaussian function (see the SI) to generate the absorption spectrum (see Figure 4). This spectrum is red-shifted by ∼70 nm (∼0.52 eV) to overlap with the experimental absorption signal observed at ∼450 nm, suspected to be from the T_1 population.[19] An identical procedure is followed after EHT is optimized in its first singlet excited state, which is similarly red-shifted by ∼70 nm. These calculated spectra support the assignment of excited-state absorption in the S_1 state (centered on ∼350 nm) and triplet state absorption in the T_1 state (centered on ∼450 nm).

From this investigation, assignment of the dynamical processes responsible for the extracted lifetimes in the global fitting procedure can be suggested. After photoexcitation to a high-lying $n^1\pi\pi^*$ state, EHT will undergo internal conversion to populate a vibrationally hot $S_1(1^1\pi\pi^*)$ state (in keeping with Kasha's rule[38] and faithfully accords with similar studies of the sunscreen constituent oxybenzone[24]), which we attribute to lifetime τ_1. We make two important remarks here: (1) Initial population of higher lying S_n states will likely lead to internal conversion within the instrument response to populate lower lying electronic states (or even S_1 directly). What τ_1 then captures will be the latter parts of the internal conversion to populate S_1 from neighboring S_n states, along with any evolution from the initial Franck−Condon window and accompanying solvent rearrangement. (2) The similarity in the DAS (τ_{1-3}) < 400 nm obtained in dioxane encourages the view that τ_1 originates principally from S_1 (or nearby states). We note such a similar comparison for the DAS extracted in methanol cannot be made owing to the positive signal around 350 (and 525 nm, see below). From here the geometry will continue to rearrange as it undergoes intramolecular vibrational relaxation within the S_1 state (given the distorted/bent nature of the optimized structure in this excited state (see Figure 4 as well as a linear interpolation of this distortion, which is given in the SI), which then couples the S_1 surface to the ground S_0 state through a $1^1\pi\pi^*/S_0$ conical intersection. Here the vibrationally hot EHT molecule cools via vibrational energy transfer (VET) to the surrounding solvent. These processes (intramolecular vibrational cooling, passage through the conical intersection, and VET) are captured by the lifetime τ_2. Contrary to what might be expected,[39] the more polar solvent methanol does not appear to contribute to a greater rate of vibrational relaxation. This can be explained by the size of EHT (126

DOI: 10.1021/acs.jpclett.7b00633
J. Phys. Chem. Lett. 2017, 8, 2113−2118

atoms; 372 vibrational modes); even with the nonpolar dioxane, EHT will likely exhibit efficient VET to the solvent given the high number of modes available. Another contribution will be the observation that EHT−methanol shows a decaying signal (centered around ∼350 nm), which rises again before decaying toward the baseline (cf. EHT-methanol TAS in Figure 2B). This feature is discussed below.

Given the observation of the long-lived absorption signals discussed (Figure 3), some of the population will become trapped on the S_1 surface, likely due to a significant geometry mismatch restricting any direct coupling to the S_0 state via the $1^1\pi\pi^*/S_0$. Instead, this population will revert to the ground state via fluorescence, suggested to be sub-600 ps from previous work.[19] Unfortunately, this fluorescence signal (which will manifest as stimulated emission) is not directly observed in the TAS, as it is likely to be buried under the convoluted triplet-state absorption and the excited-state absorption of the remaining S_1 population. In competition with the fluorescence relaxation pathway is intersystem crossing to a triplet state, which is attributed to the observed signal at ∼450 nm at Δt = 2 ns. These processes are captured by the lifetime τ_3, a time scale that would sensibly compete with the proposed fluorescence and thus populate the triplet state. Any population in this triplet state will undergo phosphorescence over a much longer time scale and thus on the time scale of this experiment manifests as a baseline offset. The lifetime given by τ_4 captures the long-lived nature of this triplet state. The broad absorption signals observed at Δt = 2 ns are also supported by these calculations, where both the S_1 and T_1 show absorption features between 350 and 450 nm, respectively.

Two further observations are made for EHT−methanol that are not seen in EHT−dioxane. (i) The first is a signal observed centered ∼525 nm in the TAS (Figure 2B), which appears concomitant with the growing signal centered around 350 nm. We suggest that these might be attributed to trapped S_1 population, which will inevitably adopt a different minimum energy geometry in the presence of the more strongly perturbing solvent methanol. Thus as the excited-state geometry evolves, the potential energy surfaces of EHT−methanol and EHT−dioxane begin to diverge due to the differences in solvent perturbation, resulting in a different transient absorption signal, as evidenced in Figure 2. As EHT−methanol approaches its minimum energy geometry in the S_1 state, it absorbs probe wavelengths centered around 525 and 350 nm; see the SI. It is important to note that these calculations remain qualitative given that solvent effects are not included, evidently resulting in optically dark transitions for trajectories (see the SI) until EHT reaches the minimum energy geometry in the S_1. Furthermore, trajectories are generated from a linear interpolation between the initial excited geometry, and the minimum energy S_1 geometry thus will not follow the minimal energy pathway along the S_1 surface (noting this pathway will also be perturbed by the solvent). These caveats might reconcile the absence of such a signal in the EHT−dioxane TAS (Figure 2A), with its presence in EHT−methanol. This signal assignment is further supported by the time scale of its appearance, much shorter than the time scale for intersystem crossing (τ_3), making triplet-state absorption an unlikely candidate for this signal. Furthermore, this feature will cause the τ_2 lifetime to extend, thus masking any increased rate of VET in methanol (vide supra). (ii) The second observation is a shorter τ_3 lifetime at ∼220 ps compared with ∼490 ps. Given the previous assignment, (i), of excited-state absorption from the S_1 minimum geometry of EHT−methanol, this observation may be explained by a potentially stronger spin−orbit coupling to the nearby triplet states(s), accelerating intersystem crossing.

To conclude, we have suggested the first complete mechanism for the photodeactivation of UV-B excited EHT, simulating its possible role in a sunscreen product. Combining ultrafast pump−probe transient absorption spectroscopy and electronic structure calculations, we have built upon previous work investigating the photophysical properties of EHT (and its analogues).[19] Given that the deactivation mechanism involves the conjugated π system at the center of EHT, this molecule, in particular, provides a stepping stone for future studies. For example, one might envision functionalizing the alkane chains of each branch of EHT to improve its chemical properties such as solubility, with little effect on its photophysical properties. On the contrary, one could alter the photophysical properties by functionalizing only the conjugated part of EHT, thereby enhancing, for example, its photostability. We hope this work serves as a stimulus for further research along both experimental and theoretical directions, which would no doubt prove fruitful.

■ ASSOCIATED CONTENT

Supporting Information

The Supporting Information is available free of charge on the ACS Publications website at DOI: 10.1021/acs.jpclett.7b00633. Data for Figures 1−4 (as well as those in the SI) are available from http://wrap.warwick.ac.uk/id/eprint/87982.

Residuals of global fits, kinetic traces, and asymptotic standard errors. Details of electronic structure calculations including: COSMO benchmark, excited state energies, and linear interpolated geometries between ground and excited states. (PDF)

■ AUTHOR INFORMATION

Corresponding Authors

*L.A.B.: E-mail: l.baker@warwick.ac.uk.

*V.G.S.: E-mail: v.stavros@warwick.ac.uk.

ORCID

Scott Habershon: 0000-0001-5932-6011

Vasilios G. Stavros: 0000-0002-6828-958X

Notes

The authors declare no competing financial interest.

■ ACKNOWLEDGMENTS

L.A.B. thanks the Engineering and Physical Sciences Research Council (EPSRC) for providing a studentship under grant EP/F500378/1, through the *Molecular Organisation and Assembly in Cells Doctoral Training Centre*. V.G.S. is grateful to the EPSRC for an equipment grant (EP/J007153) and the Royal Society and the Leverhulme Trust for a Royal Society Leverhulme Trust Senior Research Fellowship. Computing facilities were provided by the Scientific Computing Research Technology Platform of the University of Warwick.

■ REFERENCES

(1) Lowe, N. An Overview of Ultraviolet Radiation, Sunscreens, and Photo-Induced Dermatoses. *Dermatol. Clin.* **2006**, *24*, 9−17.

(2) Urbach, F. The historical aspects of sunscreens. *J. Photochem. Photobiol., B* **2001**, *64*, 99−104.

DOI: 10.1021/acs.jpclett.7b00633
J. Phys. Chem. Lett. 2017, 8, 2113−2118

(3) Siegel, R. L.; Miller, K. D.; Jemal, A. Cancer Statistics. *Ca-Cancer J. Clin.* **2016**, *66*, 7−30.
(4) Lucas, R.; McMichael, T.; Smith, W.; Armstrong, B. *Solar Ultraviolet Radiation. Global Burden of Disease from Solar Ultraviolet Radiation*; Environmental Burden of Disease Series *13*; World Health Organization: Geneva, 2006.
(5) Baker, L. A.; Stavros, V. G. Observing and Understanding the Ultrafast Photochemistry in Small Molecules: Applications to Sunscreens. *Sci. Prog.* **2016**, *99*, 282−311.
(6) Kasparian, N. A.; McLoone, J. K.; Meiser, B. Skin cancer-related prevention and screening behaviors: a review of the literature. *J. Behav. Med.* **2009**, *32*, 406−428.
(7) Lodén, M.; Beitner, H.; Gonzalez, H.; Edström, D.; Åkerström, U.; Austad, J.; Buraczewska-Norin, I.; Matsson, M.; Wulf, H. Sunscreen use: controversies, challenges and regulatory aspects. *Br. J. Dermatol.* **2011**, *165*, 255−262.
(8) Burnett, M. E.; Wang, S. Q. Current sunscreen controversies: a critical review. *Photodermatol., Photoimmunol. Photomed.* **2011**, *27*, 58−67.
(9) Jansen, R.; Osterwalder, U.; Wang, S. Q.; Burnett, M.; Lim, H. W. Photoprotection Part II. Sunscreen: Development, efficacy, and controversies. *J. Am. Acad. Dermatol.* **2013**, *69*, 867.e1−867.e14.
(10) Mancebo, S. E.; Hu, J. Y.; Wang, S. Q. Sunscreens: A Review of Health Benefits, Regulations, and Controversies. *Dermatol. Clin.* **2014**, *32*, 427−438.
(11) Shaath, N. A. Ultraviolet filters. *Photochem. Photobiol. Sci.* **2010**, *9*, 464−469.
(12) Baker, L. A.; Greenough, S. E.; Stavros, V. G. A Perspective on the Ultrafast Photochemistry of Solution-Phase Sunscreen Molecules. *J. Phys. Chem. Lett.* **2016**, *7*, 4655−4665.
(13) Baker, L. A.; Marchetti, B.; Karsili, T. N. V.; Stavros, V. G.; Ashfold, M. N. R. Photoprotection: extending lessons learned from studying natural sunscreens to the design of artificial sunscreen constituents. *Chem. Soc. Rev.* **2017**, In press.
(14) Hunter, J. D. Matplotlib: A 2D graphics environment. *Comput. Sci. Eng.* **2007**, *9*, 90−95.
(15) González, S.; Fernández-Lorente, M.; Gilaberte-Calzada, Y. The latest on skin photoprotection. *Clin. Dermatol.* **2008**, *26*, 614−626.
(16) Herzog, B.; Wehrle, M.; Quass, K. Photostability of UV Absorber Systems in Sunscreens. *Photochem. Photobiol.* **2009**, *85*, 869−878.
(17) Lhiaubet-Vallet, V.; Marin, M.; Jimenez, O.; Gorchs, O.; Trullas, C.; Miranda, M. A. Filter-filter interactions. Photostabilization, triplet quenching and reactivity with singlet oxygen. *Photochem. Photobiol. Sci.* **2010**, *9*, 552−558.
(18) Sommer, S.; Wilkinson, S. M.; English, J. S. C.; Ferguson, J. Photoallergic contact dermatitis from the sunscreen octyl triazone. *Contact Dermatitis* **2002**, *46*, 304−305.
(19) Tsuchiya, T.; Kikuchi, A.; Oguchi-Fujiyama, N.; Miyazawa, K.; Yagi, M. Photoexcited triplet states of UV-B absorbers: ethylhexyl triazone and diethylhexylbutamido triazone. *Photochem. Photobiol. Sci.* **2015**, *14*, 807−814.
(20) Grubb, M. P.; Orr-Ewing, A. J.; Ashfold, M. N. R. KOALA: A program for the processing and decomposition of transient spectra. *Rev. Sci. Instrum.* **2014**, *85*, 064104.
(21) Greenough, S. E.; Roberts, G. M.; Smith, N. A.; Horbury, M. D.; McKinlay, R. G.; Żurek, J. M.; Paterson, M. J.; Sadler, P. J.; Stavros, V. G. Ultrafast photo-induced ligand solvolysis of cis-[Ru(bipyridine)$_2$(nicotinamide)$_2$]$^{2+}$: experimental and theoretical insight into its photoactivation mechanism. *Phys. Chem. Chem. Phys.* **2014**, *16*, 19141−19155.
(22) Baker, L. A.; Horbury, M. D.; Greenough, S. E.; Coulter, P. M.; Karsili, T. N. V.; Roberts, G. M.; Orr-Ewing, A. J.; Ashfold, M. N. R.; Stavros, V. G. Probing the Ultrafast Energy Dissipation Mechanism of the Sunscreen Oxybenzone after UVA Irradiation. *J. Phys. Chem. Lett.* **2015**, *6*, 1363−1368.
(23) Chatterley, A. S.; West, C. W.; Stavros, V. G.; Verlet, J. R. R. Time-resolved photoelectron imaging of the isolated deprotonated nucleotides. *Chem. Sci.* **2014**, *5*, 3963−3975.
(24) Baker, L. A.; Horbury, M. D.; Greenough, S. E.; Ashfold, M. N. R.; Stavros, V. G. Broadband ultrafast photoprotection by oxybenzone across the UVB and UVC spectral regions. *Photochem. Photobiol. Sci.* **2015**, *14*, 1814−1820.
(25) Baker, L. A.; Horbury, M. D.; Greenough, S. E.; Allais, F.; Walsh, P. S.; Habershon, S.; Stavros, V. G. Ultrafast Photoprotecting Sunscreens in Natural Plants. *J. Phys. Chem. Lett.* **2016**, *7*, 56−61.
(26) Hockett, P. General discussion. *Faraday Discuss.* **2013**, *163*, 513−543.
(27) Baker, L. A.; Horbury, M. D.; Stavros, V. G. Ultrafast photoprotective properties of the sunscreening agent octocrylene. *Opt. Express* **2016**, *24*, 10700−10709.
(28) Humphrey, W.; Dalke, A.; Schulten, K. VMD − Visual Molecular Dynamics. *J. Mol. Graphics* **1996**, *14*, 33−38.
(29) TURBOMOLE V7.0 2015, A development of University of Karlsruhe and Forschungszentrum Karlsruhe GmbH, 1989−2007, TURBOMOLE GmbH, since 2007; available from http://www.turbomole.com.
(30) von Arnim, M.; Ahlrichs, R. Performance of Parallel TURBOMOLE for Density Functional Calculations. *J. Comput. Chem.* **1998**, *19*, 1746−1757.
(31) Perdew, J. P. Density-functional approximation for the correlation energy of the inhomogeneous electron gas. *Phys. Rev. B: Condens. Matter Mater. Phys.* **1986**, *33*, 8822−8824.
(32) Dunning, T. H. Gaussian basis sets for use in correlated molecular calculations. I. The atoms boron through neon and hydrogen. *J. Chem. Phys.* **1989**, *90*, 1007−1023.
(33) Kendall, R. A.; Dunning, T. H.; Harrison, R. J. Electron affinities of the first-row atoms revisited. Systematic basis sets and wave function. *J. Chem. Phys.* **1992**, *96*, 6796−6806.
(34) Eichkorn, K.; Treutler, O.; Öhm, H.; Häser, M.; Ahlrichs, R. Auxiliary basis sets to approximate Coulomb potentials. *Chem. Phys. Lett.* **1995**, *240*, 283−290.
(35) Sierka, M.; Hogekamp, A.; Ahlrichs, R. Fast evaluation of the Coulomb potential for electron densities using multipole accelerated resolution of identity approximation. *J. Chem. Phys.* **2003**, *118*, 9136−9148.
(36) Eichkorn, K.; Weigend, F.; Treutler, O.; Ahlrichs, R. Auxiliary basis sets for main row atoms and transition metals and their use to approximate Coulomb potentials. *Theor. Chem. Acc.* **1997**, *97*, 119−124.
(37) Klamt, A.; Schüürmann, G. COSMO: a new approach to dielectric screening in solvents with explicit expressions for the screening energy and its gradient. *J. Chem. Soc., Perkin Trans. 2* **1993**, *2*, 799−805.
(38) Kasha, M. Characterization of electronic transitions in complex molecules. *Discuss. Faraday Soc.* **1950**, *9*, 14−19.
(39) Owrutsky, J. C.; Raftery, D.; Hochstrasser, R. M. Vibrational Relaxation Dynamics in Solutions. *Annu. Rev. Phys. Chem.* **1994**, *45*, 519−555.

DOI: 10.1021/acs.jpclett.7b00633
J. Phys. Chem. Lett. 2017, 8, 2113−2118